

Lawrence Berkeley National Laboratory

Lawrence Berkeley National Laboratory

Title

Detection of Fatigue Damage Prior to Crack Initiation with Scanning SQUID Microscopy

Permalink

<https://escholarship.org/uc/item/0rd6s6qw>

Authors

Lee, Tae-Kyu
Morris Jr., J.W.
Lee, Seungkyun
[et al.](#)

Publication Date

2005-11-07

Peer reviewed

DETECTION OF FATIGUE DAMAGE PRIOR TO CRACK INITIATION WITH SCANNING SQUID MICROSCOPY

Tae-Kyu Lee¹, J.W.Morris, Jr.¹, Seungkyun Lee² and John Clarke²

¹Department of Materials Science & Engineering, ²Department of Physics
University of California, Berkeley, and
Materials Science Division, Lawrence Berkeley National Laboratory, Berkeley, CA 94720

ABSTRACT. The remanence fields of fatigued ferritic steel specimens were measured using a scanning microscope based on a high transition temperature Superconducting Quantum Interference Device (SQUID). The results show an overall increase of remanence until dislocation density saturates and an additional local remanence increase after saturation during cyclic loading. Because of the combined magnetic and spatial resolution of the SQUID microscope, these local changes of dislocation structures can be detected before a crack actually initiates, and identify the sites where crack nucleation will occur.

Keywords: Non-destructive evaluation, Fatigue, Superconducting Quantum Interference Device (SQUID), Dislocation, Microcrack, **PACS:** 07.55.Ge, 62.20.Mk, 74.81.Fa, 75.60.Ej, 62.20.Fe

INTRODUCTION

The fatigue process can be detected and monitored in the earliest stages of high-cycle fatigue, by the increase in dislocation density and hardness, and in the final stages, through the direct observation of initiated cracks [1-3]. But there are no probative, non-destructive techniques to follow incipient fatigue through the critical intermediate stage between dislocation saturation and prior to crack nucleation. In earlier studies, we reported initial success in using SQUID microscopy for this purpose [4,5]. It is the magnetostrictive coupling (and also the magnetostatic coupling if the defects are larger than the thickness of domain walls) between the structural defects and the domain walls that affect the movement of the domain walls and therefore the ferromagnetic properties. The discontinuous motion of domain walls in ferromagnetic materials due to the interaction with defects generates bursts of magnetic induction [6-10]. Dislocations and microcracks act as pinning sites that impede the motion of magnetic domain walls under an applied magnetic field. Subtle changes in local magnetic behavior follow the reconfiguration of defects that occurs in the intermediate stages of fatigue, which can be detected by mapping the local remanence field of a fatigued specimen. The interaction of magnetic domains and microstructural defects have the potential to provide detailed information of the material of interest in a non-destructive way.

EXPERIMENTAL PROCEDURE

Ferritic stainless steel (AISI430) plate tensile specimens with a 40mm gauge length and 5mm width were used in this study. The chemical composition was Fe-16Cr-1Mn-1Si-0.04P-0.03S-0.12C (wt%). The specimens were annealed at 1100°C for 2 hours to relieve any stress that remained from machining, then cooled by slow, controlled furnace cooling (FC) which resulted in fully ferritic microstructure with an average grain size of $\sim 30\mu\text{m}$. The measured yield and tensile strengths were 312MPa and 489MPa, respectively. The samples were fatigued in a tension-tension cycle under load control with a frequency of 5Hz, at room temperature in ambient air. The stress cycle range was from near zero to 90% of the yield strength: 30MPa to 250MPa.

The scanning SQUID microscope used in this study was developed in the Department of Physics, University of California, Berkeley, and is based on a high- T_c DC-SQUID [11,12]. The SQUID (Superconducting QUantum Interference Device) is a very sensitive detector of changes in magnetic field. Its essential element is a superconducting loop with two Josephson junctions. Figure 1 shows a schematic drawing of the SQUID microscope. The high- T_c DC-SQUID chip is placed on top of a sapphire rod, which is thermally coupled to a liquid nitrogen reservoir. The SQUID chip is thermally isolated by a 300 μm separation from a 125 μm thick sapphire window in a vacuum chamber. The sample stage is placed on a brass table attached to an aligned x-y translation stage, which is operated by two stepper motors. A detailed description of this SQUID microscope can be also found in references [13] and [14]. This design makes it possible to scan a sample at room temperature by placing it in close proximity to the SQUID. The scanning is controlled by stepper motors, and produces a two-dimensional magnetic field image that combines high magnetic resolution with high spatial resolution. Thus, it is a sensitive technique to detect the precise locations and quantitative details of defects and microstructural changes.

In the experiments described here fatigued samples are unloaded during the fatigue process after certain loading cycles, demagnetized, and magnetized in a uniform 50mT magnetic field. In addition to those samples, three separate specimens are prepared with an initial hardness of around 180H_{v400}, to observe and compare the remanence data with the hardness increase during cyclic loading, and a series of fatigue specimens were prepared for TEM analysis.

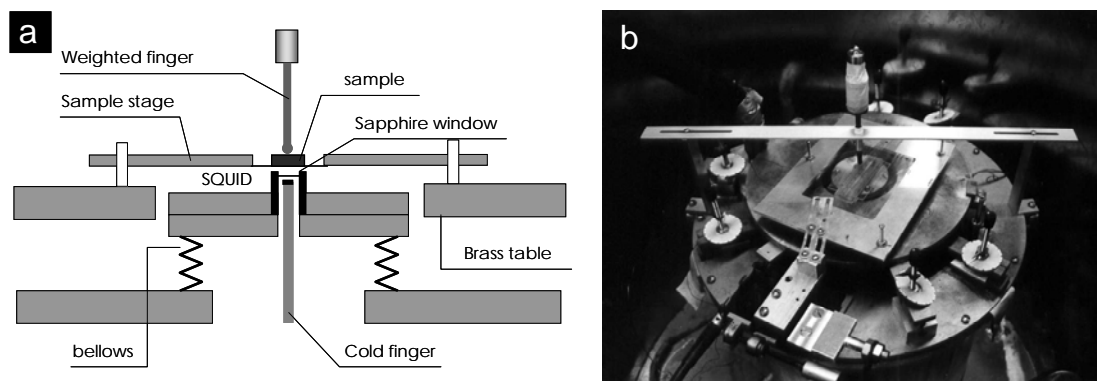


FIGURE 1. (a) Schematics of the close up of the SQUID microscope near SQUID chip. (b) Photo of the SQUID microscope.

RESULTS AND DISCUSSION

Figure 2 shows the development of the remanent magnetization patterns as a function of fatigue cycles. The measurement was applied to the middle of the specimen with a $10 \times 20 \text{ mm}^2$ scanning area. The magnetization tends to increase with the number of fatigue cycles and the overall magnetization develops a pronounced pattern with local peaks in particular locations along the sample edge. Especially, a localized high intensity region is formed after 2×10^4 cycles which is indicated as **A(SS-4)** (Figure 2(d)).

Figure 3 shows the maximum intensity points of the right side edge measurement. A sharp increase of a local peak is observed after 12×10^4 cycles, which indicates fatigue damage development. After 28×10^4 cycles, the profile shows a secondary local peak. With 15×10^3 additional fatigue cycles after 92×10^4 cycles, a total fracture occurred but still no crack was observed at region **A(SS-4)**. A gradual polishing of the surface revealed a microcrack after a third step reduction (one step: $50\text{-}100 \mu\text{m}$) as shown in Figure 3(b).

When we combine the remanence magnetization at regions **A(SS-4)** with the measured microhardness as a function of the fatigue cycle number, the plot appears as Figure 4, where the last hardness point was obtained from the magnetically scanned specimen directly. A continuous increase of the remanence is observed followed by a steep increase after approximately 90×10^4 cycles, the fatigue cycle number when the first surface crack was observed.

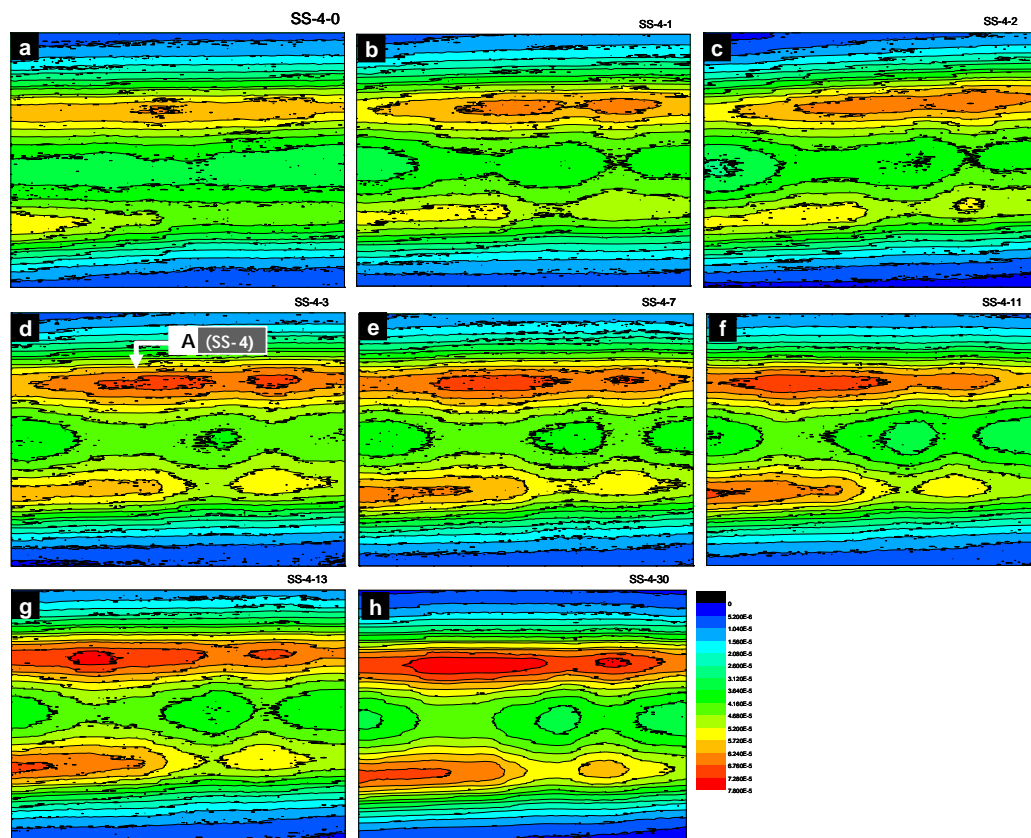


FIGURE 2. Remanent magnetization map of 430 stainless steel SS-4 sample after (a) 0 (b) 1×10^3 (c) 5×10^3 (d) 2×10^4 (e) 12×10^4 (f) 14.5×10^4 (g) 28×10^4 and (h) 92×10^4 cycles. Scanning area $10 \text{ mm} \times 20 \text{ mm}$.

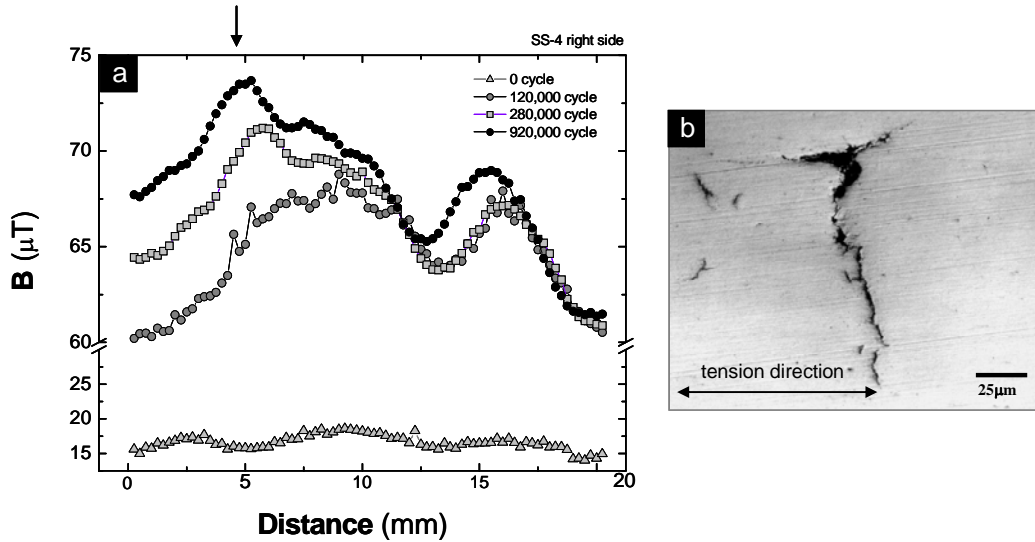


FIGURE 3. (a) Maximum remanent magnetization intensity profile of 430 stainless steel sample SS-4, right side of the sample. (The area indicated by the arrow is the same as that at A(SS-4) in Fig 3(d).) (b) Optical micrograph of microcracks at A(SS-4) after step polishing.

We have attempted to categorize the magnetic measurements taken during cyclic loading to define sequential steps in the fatigue process. The first stage of fatigue lasts for the first 1×10^4 cycles, where the dislocation density increase causes an increase in hardness from $180H_{v400}$ to $320H_{v400}$. This increase in dislocation density also causes a significant increase in magnetic domain wall pinning in the first stage; the overall remanent magnetization value increased from $20\mu T$ to $55\sim 65\mu T$. In the second stage of fatigue the remanence increases further due to a mixture of several localized events such as additional dislocation density increase, dislocation distribution or cell formation and the formation of small cracks. There is little change in the overall hardness; the major cause of the remanence increase during the second stage appears to be due to factors such as the dislocation distribution or cell formation and formation of small cracks.

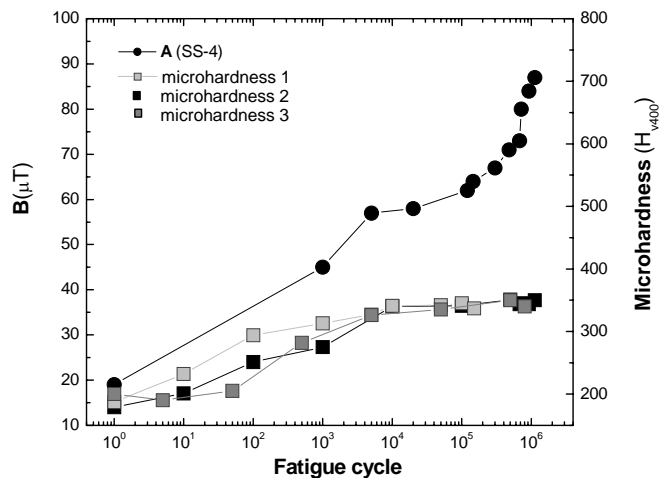


FIGURE 4. Remanence intensity value at A(SS-4) with microhardness as a function of fatigue cycle number.

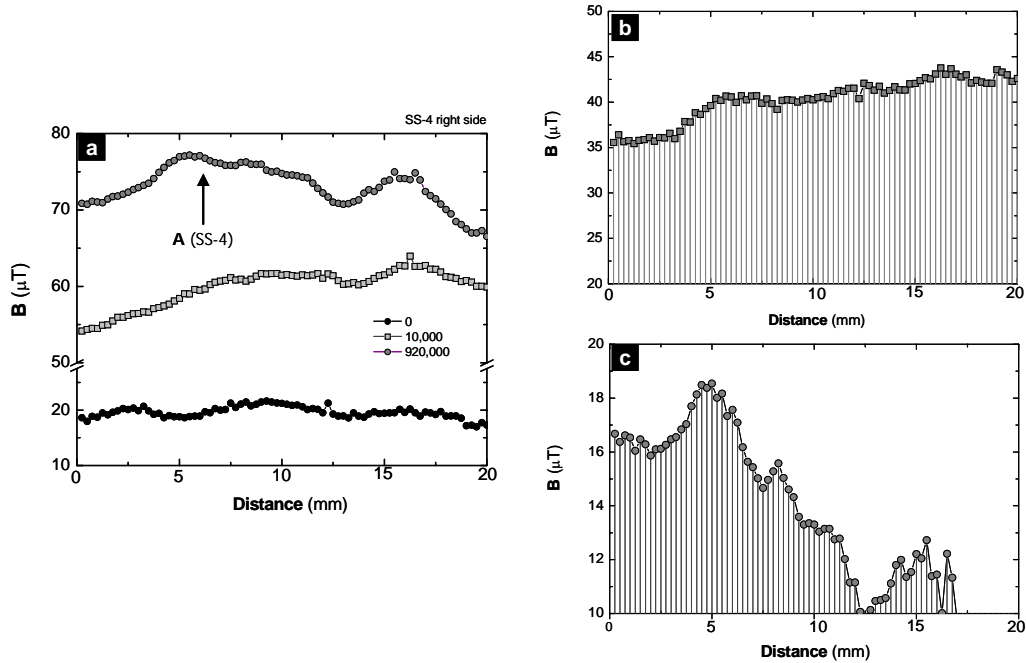


FIGURE 5. (a) Remanence maximum intensity profile of right side of 430 stainless steel sample SS-4 after 0, 1×10^4 , and 92×10^4 cycles. (b) Remanence development during 0 to 1×10^4 cycles, (c) remanence development after dislocation density saturation.

By using the remanent magnetization profile at 0, 1×10^4 and at the final measurement from Figures 2 and 3(a), we can distinguish the remanent magnetization intensity from the first and second steps. The remanence caused by the dislocation density increase can be plotted as in Figure 5. The remanence profile after 1×10^4 cycles can be subtracted to isolate subsequent changes. The overall increase of the intensity shows a remanence value around $40 \mu\text{T}$. When we subtract the 1×10^4 cycle remanence profile from the remanence profile after 92×10^4 cycles, the last measured remanence intensity where the crack was observed after step polishing, the remanence has the profile shown in Figure 5(c). This profile represents the remanence which was developed after the dislocation density was saturated, and thus was produced by factors other than the dislocation density increase.

Figure 6 shows the TEM microstructure after 1×10^3 , 1×10^4 , 2×10^4 , 40×10^4 and 50×10^4 fatigue cycles. A series of specimens was prepared using the same heat treatment as for the SS-4 furnace cooled specimen. To obtain a TEM sample after a certain number of fatigue cycles, specimens were fatigued with the same stress range, 30MPa-250MPa, and cut in the middle after confirming that the cut area showed the same remanent magnetization value as specimen SS-4 for the same number of fatigue cycles. Five specimens were prepared from each condition. A series of TEM observation was performed and a dominant microstructure was selected and taken as the representative dislocation structure after the given number of fatigue cycles. The dislocation structure shows a constant increase of dislocation density where an increase of hardness was measured. In several references [15,16], the saturation of the dislocation density is reported in the range of a few hundred cycles, but in these series of specimens both the measured hardness and the TEM microstructure shows the tendency of saturation after approximately 1×10^4 cycles.

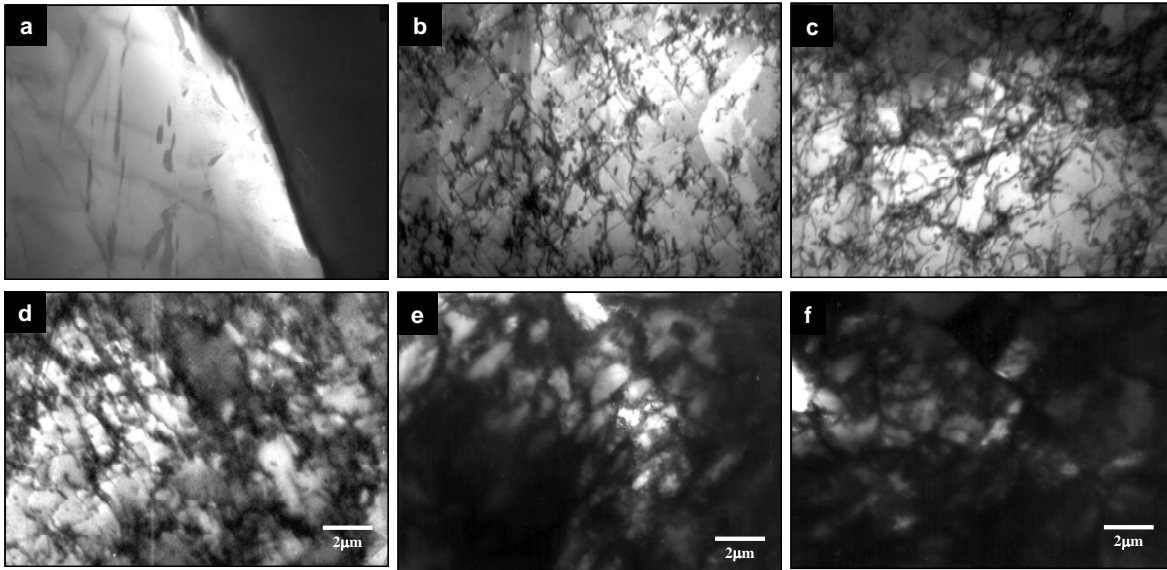


FIGURE 6. TEM microstructure of fatigued furnace cooled 430 stainless steel after (a) 0 cycle (b) 1×10^3 (c) 1×10^4 (d) 2×10^4 (e) 40×10^4 and (f) 50×10^4 cycles.

The first hundred cycles lead to a considerable increase in dislocation density, distributed more or less homogeneously. After 1×10^3 cycles, the dislocations seem to form denser areas called bands or patches, and the areas between the bands show a much lower dislocation density. After 1×10^4 fatigue cycles, the randomly distributed dislocations begin to show a stabilized dislocation cell structure and after 50×10^4 fatigue cycles, the cell structure shows a dislocation cell with an average diameter of $\sim 3 \mu\text{m}$, where the wall of dislocation cells became denser and the inner part of the dislocation cell has a lower density of dislocations.

Based on this observation the remanence increase after dislocation density saturation, which is shown in Figure 5(c), can be explained by the formation and stabilization of the dislocation cell structure. When we combine the observations and possible explanations of the fatigued process of the furnace cooled 430 ferritic stainless steel specimen, we can summarize those in a plot as shown in Figure 7.

At the first stage of fatigue, an increase of dislocation density occurs. These increased dislocations pin the domain walls during magnetization and provide an overall development of remanence until the number of dislocations no longer increases. It is at the saturation stage where the dislocation structure shows an equilibrium between the generation and annihilation of dislocations. Therefore, the dislocation cell structure begins to stabilize, and no additional dislocation density increase occurs. During this second fatigue stage, the distance between dislocations in cell walls decreases. These tightened cell walls provide stronger domain wall pinning sites and resulted in a further increase of remanence. In contrast to the first fatigue stage, the remanent magnetization field increase occurs locally. Local peaks begin to appear with a higher intensity than the overall increase which occurs at the first stage. At approximately 90% of the material's fatigue life, a microcrack begins to occur and a steep increase of remanence is observed at the locally developed intensity peaks. A schematic drawing of the remanence increase along the gauge area is presented in Figure 7(b).

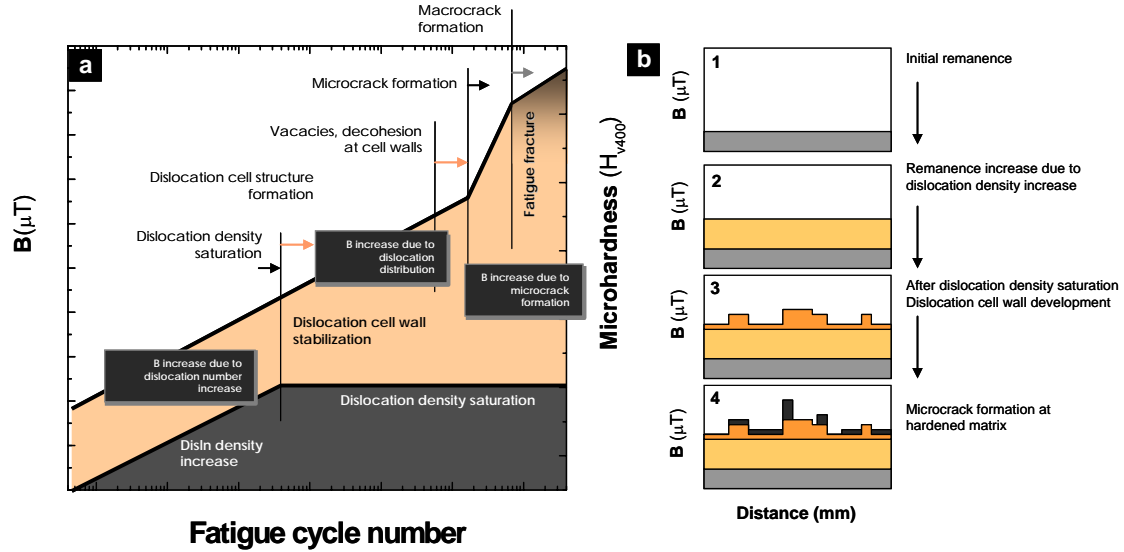


FIGURE 7. Reconstruction of remanent magnetization diagram as a function of fatigue cycle number. (b) Schematic drawing of remanence development during cyclic loading at the gauge area.

CONCLUSION

One important unique observation through this scanning SQUID microscopy is the local remanence increase after the dislocation density saturation is reached. Compared to the total fatigue life time $\sim 1 \times 10^6$, the dislocation density saturation occurs after 1×10^4 cycles, which is approximately at 1% of the total lifetime. And as shown in Figure 3(a), locally developed remanence peaks were observed at 10% of the fatigue lifetime, with more localized secondary peaks at 20% of the total lifetime. This localized remanence peak is the location where a microcrack was observed. Based on these results, we can say that the possible location where the microcrack will initiate can be detected at 10-20% of the sample's fatigue lifetime using highly sensitive, high spatial resolution scanning SQUID microscopy. Thus, this technique is able to detect fatigue damage prior to crack initiation.

ACKNOWLEDGMENT

This work was supported by the Director, Office of Science, Office of Basic Energy Sciences, Materials Sciences and Engineering Division, of the U.S. Department of Energy under Contract No. DE-AC02-05CH11231.

REFERENCES

1. M. Klesnil, P. Lukas, *Fatigue of Metallic Materials*, Elsevier, New York, 1992, p.14.
2. D.C. Jiles, *NDT International*, 21, 1988, p.311.
3. T. Erber, S.A. Guralnick, R.D. Desai, and W. Kwok, *J. Phys. D: Appl. Phys.* **30**, p.2818 (1997).

4. Tae-Kyu Lee, D.M. Clatterbuck, J.W. Morris, Jr., T.J. Shaw, SeungKyun Lee, and J. Clarke, in *Review of Quantitative Nondestructive Evaluation*, eds. D.O. Thompson and D.E. Chimenti (Plenum, New York, 21, 2002), p.453.
5. D.M. Clatterbuck, Tae-Kyu Lee, T.J. Shaw, N.F. Heinig, John Clarke, and J.W. Morris, Jr., *IEEE Trans. Appl. Supercond.* **11**, p.1307 (2001).
6. H. Weinstock, *IEEE Trans. Magn.* **27**, p.3231 (1991).
7. Y. Bergstorm, O. Vingsbo, *Mat. Sci.Eng.* **6**, p.150 (1969).
8. J. Banchet, J. Jouglar, P.-L. Vuillermoz, P. Waltz, and H. Weinstock, in *Review of Progress in Quantitative Nondestructive Evaluation*, eds. D.O. Thompson and D.E. Chimenti (Plenum, New York, 14, 1995), p.1675.
9. J. Banchet, J. Jouglar, P.-L. Vuillermoz, P. Waltz, and H. Weinstock, *IEEE Trans. Appl. Supercond.* **5**, p.2486 (1995).
10. M. Lang, J. Johnson, J. Schreiber, G. Dobmann, H.-J. Bassler, D. Eifler, R. Ehrlich, and U. Gampe, *Nuclear Eng. and Design*, **198**, p.185 (2000).
11. T.J. Shaw, K. Schlenga, R. McDermott, John Clarke, J. W. Chan, S.-H. Kang, and J.W. Morris, Jr., *IEEE Trans. Appl. Supercond.* **9**, p.4107 (1999).
12. T.S. Lee, G. Dantsker, and John Clarke, *Rev. Sci. Inst.* **67**, p.4208 (1996).
13. T.J. Shaw, J.W. Chan, S.-H. Kang, R. McDermott, J.W. Morris, Jr., and John Clarke, *Acta Mat.* **48**, p.2655 (2000).
14. J.W. Chan, J.W. Morris, Jr., T.J. Shaw, K. Schlenga, D.D. Graca, D. Sterry, and J. Clarke, in *Nondestructive Evaluation and Material Properties*, eds. R.J. Arsenault and P.K. Liaw (TMS, 1999), p.29.
15. P. Lukas, and M. Klesnil, *Czech. J. Phys.*, B15, p.600 (1964).
16. P. Lukas, M. Klesnil, and P. Rys, *Z. Metallknde.* **56**, p.109 (1965).